

Pre-emptive parametric kill switch for evaporative atomic sources in vacuum

Shuang Li(李爽), Zhiyuan Lin(林志远), Sen Li(李森), Mohan Zhang(张默含), Fengquan Zhang(张凤泉), Jin Hu(胡瑾), Xiaotong Liu(刘宵彤), Lin Meng(孟林), Tim Byrnes, and Valentin Ivannikov(瓦伦丁)

Citation: Chin. Phys. B, 2026, 35 (**7**): 073701. DOI: 10.1088/1674-1056/ae577f
http://cpb.iphy.ac.cn; http://iopscience.iop.org/cpb

What follows is a list of articles you may be interested in

Compact dual MOT apparatus of K and Rb for optical tweezer experiment

Kedi Wei(魏可迪), Yangbo Wei(韦样波), Shangjin Li(李上进), and Bo Yan(颜波)

Chin. Phys. B, 2026, 35 (**1**): 013701. DOI: 10.1088/1674-1056/ade8e2

A Rb-Cs dual-species magneto-optical trap

Shiyao Shao(邵师尧), Qing Li(李庆), Lihua Zhang(张力华), Bang Liu(刘邦), Zhengyuan Zhang(张正源), Qifeng Wang(王启锋), Jun Zhang(张俊), Yu Ma(马宇), Tianyu Han(韩天宇), Hanchao Chen(陈瀚超), Jiadou Nan(南佳豆), Yiming Yin(殷一鸣), Dongyang Zhu(朱东杨), Yajun Wang(王雅君), Dongsheng Ding(丁冬生), and Baosen Shi(史保森)

Chin. Phys. B, 2025, 34 (**6**): 063702. DOI: 10.1088/1674-1056/adc190

Observation of momentum-induced broadening of width in narrow Feshbach resonances of ultracold ^{133}Cs atoms

Zhennan Liu(刘震南), Hongxing Zhao(赵宏星), Yunfei Wang(王云飞), Yuqing Li(李玉清), Jizhou Wu(武寄洲), Wenliang Liu(刘文良), Peng Li(李鹏), Yongming Fu(付永明), Liantuan Xiao(肖连团), Jie Ma(马杰), and Suotang Jia(贾锁堂)

Chin. Phys. B, 2025, 34 (**2**): 023701. DOI: 10.1088/1674-1056/ad92fc

Compact magneto-optical traps using planar optics

Zhi Tan(谭智), Bo Lu(鹿博), Chengyin Han(韩成银), and Chaohong Lee(李朝红)

Chin. Phys. B, 2024, 33 (**9**): 093701. DOI: 10.1088/1674-1056/ad607a

Off-site trimer superfluid on a one-dimensional optical lattice

Er-Nv Fan(范二女), Tony C Scott, Wan-Zhou Zhang(张万舟)

Chin. Phys. B, 2017, 26 (**4**): 043701. DOI: 10.1088/1674-1056/26/4/043701

INSTRUMENTATION AND MEASUREMENT

Pre-emptive parametric kill switch for evaporative atomic sources in vacuum

Shuang Li(李爽)[1,2,†], Zhiyuan Lin(林志远)[1,2,†], Sen Li(李森)[1,2], Mohan Zhang(张默含)[1,2], Fengquan Zhang(张凤泉)[1,2], Jin Hu(胡瑾)[1,2], Xiaotong Liu(刘宵彤)[1,2], Lin Meng(孟林)[1,2], Tim Byrnes[1,2,3,4,5,‡], and Valentin Ivannikov(瓦伦丁)[2,§]

[1] *State Key Laboratory of Precision Spectroscopy, School of Physical and Material Sciences, East China Normal University (ECNU), Shanghai* 200062, *China*
[2] *New York University (NYU) Shanghai, Shanghai* 200126, *China*
[3] *NYU-ECNU Institute of Physics at NYU Shanghai, Shanghai* 200062, *China*
[4] *Center for Quantum and Topological Systems, New York University Abu Dhabi (NYUAD) Research Institute, NYUAD, UAE*
[5] *Department of Physics, New York University, New York, NY* 10003, *USA*

(Received 9 December 2025; revised manuscript received 18 March 2026; accepted manuscript online 26 March 2026)

A robust pre-emptive kill switch for cold atom experiments is introduced to significantly reduce costly system reassembly or replacement. The design incorporates upper (alarm) and lower (evaporation) event detection mechanisms based on predefined thresholds. Meanwhile, a duty cycle timing methodology is employed to prevent unintentional activation of the dispenser when pulse signals occur. The circuit employs generic components, a modular design, and formalized logic, ensuring cost-effectiveness and making the design suitable for school laboratories and other research environments. This design is highly versatile and can be applied to other sensitive devices beyond dispensers, such as heating filaments, titanium sublimation pumps, tungsten lamps, and comparable systems.

Keywords: cold atom experiment, alkali metal dispenser, dispenser protection mechanism, vacuum technology

PACS: 37.10.De, 07.30.Kf, 07.77.Gx, 84.30.–r

DOI: 10.1088/1674-1056/ae577f **CSTR:** 32038.14.CPB.ae577f

1. Introduction

Alkali metal vapors are a vital resource for numerous emerging chip-scale quantum technologies, such as atomic clocks,[1,2] quantum gravimeters,[3,4] and quantum computers,[5,6] which are increasingly attractive for the implementation of new quantum device architectures.[7,8] The sharp resonances of alkali atoms find applications in atom cooling, precision spectroscopy, and the frequency stabilization of lasers on atomic transitions.[9,10] A source of (warm) alkali atoms is required in all cold-atom systems to provide an appropriate atom density for forming the magneto-optic trap (MOT),[11–15] as the appropriate atom density significantly determines the characteristics of the MOT, such as the load rate, loading time, loss rate, and cooling beam intensity. However, an inappropriate density may even destroy MOT trapping.[16] Light-induced atom desorption (LIAD) from cell surfaces has been investigated to modulate atom density.[9,17–22] Although it performs well in some experiments, reproducibility issues may occur, and such methods have yet to be miniaturized to facilitate portability and microfabrication.[23,24]

There exists a wide range of methods to produce dilute atomic gases for alkaline, alkaline earth, rare earth, and other metals with low or moderate melting points.[25–29] It is even possible to prepare vapors of more exotic metals that are particularly difficult to evaporate, such as Zr, Nb, Mo, Ta, and W, by the dissociation of chemical compounds containing these metal atoms.[30] Commercial alkali-metal dispensers (e.g., Li, Na, K, Rb, Cs) have been widely used in laboratory-based cold-atom experiments for decades because they keep the background pressure low while providing many atoms for trapping.[31,32] Another advantage of using a metal dispenser over more traditional atom sources in cold-atom experiments is that the dispenser can be used directly in an ultrahigh vacuum (UHV) environment.[33] Typically, the dispenser produces a controllable source of alkali-metal atom vapor emission into the UHV through evaporation during ohmic heating. The operation of the heater with a current in the range of 3–7 A heats the dispenser to a temperature range of 400–800 °C.[25,28,34] We do not directly measure the dispenser temperature, even though such measurements are tempting and we indeed have a thermocouple directly attached to the dispenser in situ, because temperature measurements are typically completed on the scale of the critical reaction time or slower, making such metrology inadequate for failure prevention. In con-

[†]These authors contributed equally to this work.
[‡]Corresponding author. E-mail: tim.byrnes@nyu.edu
[§]Corresponding author. E-mail: valentin@nyu.edu

© 2026 Chinese Physical Society and IOP Publishing Ltd. All rights, including for text and data mining, AI training, and similar technologies, are reserved.

trast, electrical current measurements are instantaneous. If the dispenser exposure is limited to a capped current over a specified time, the maximal energy allowed to be dissipated by the dispenser in a single run is effectively limited to $T_{\max} \cdot I^2 \cdot R_{\mathrm{d}}$, where I is the current, R_{d} is the dispenser resistance, and $T_{\max}$ is the longest allowed operation duration.[35] The dissipated power is monotonically related to the temperature, providing a way to exploit instantaneous current measurements to estimate the temperature dynamics with sufficient accuracy for regulatory purposes.

However, dispenser systems are characterized by complex nonlinear dynamics as a result of their open dissipative nature, making them vulnerable to instabilities that may induce hazardous conditions or equipment malfunctions. One such instability is exponential thermal runaway, which can result in dispenser burnout, a prevalent failure mechanism in titanium sublimation pumps and vacuum gauges, ultimately leading to significant system failures. Therefore, the development of a robust kill switch for these sensitive devices is imperative to minimize the expensive system reassembly or replacement that often causes substantial time losses.

Although traditional proportional-integral-derivative (PID) regulators, based on the principle of proportional-integral-derivative control, are widely used to achieve continuous regulation, they have shown deficiencies when dealing with sudden transitions (such as power transistor failures), which may put the system in a dangerous state. Furthermore, improper adjustment of PID parameters can exacerbate instability and cause the system to deviate further from the safe state. Therefore, using PID control alone cannot ensure reliable protection for these sensitive components. For example, similar mechanisms have been applied in modern battery systems, such as those in mobile phones, to prevent overcharging and extend battery life. These systems sometimes limit a full charge and stop at the 80% level, then continue charging after a while. The prohibition of secondary activation under such conditions demonstrates an overcharge prevention approach that aligns conceptually with our design. Moreover, battery management systems employ battery negative current (BNC) and battery minus current (BMC) modules to monitor and disconnect current through battery terminals when a threshold is exceeded, preventing the risk of overcurrent.[36–39] Consequently, an auxiliary protection mechanism is necessary to bridge this gap and ensure that the system transitions to an unequivocally safe state under all conditions.

In this study, we developed a reliable kill switch utilizing LTspice simulation, which was subsequently corroborated by building a physical prototype. The design ensures that the active state of the dispenser is safeguarded by implementing current limiters to maintain operation within the prescribed current range. Meanwhile, we devised a duty cycle timing strategy to prevent the dispenser from accidentally starting after receiving a pulse signal. This circuit serves as a quasi-DC safety mechanism, continuously monitoring the current and cutting off the current when it exceeds the set power-loss parameters (including the maximum current and specific operating time limit). This method effectively limits the total power loss, thereby avoiding serious faults such as thermal runaway.

2. Design overview

This pre-emptive parametric kill switch was designed to regulate the alkali metal dispenser exposure through current limitation and ensure precise activation timing. As shown in Fig. 1, the operational condition of the load is governed by two control loops: PID CONTROL LOOP and PROTECTOR CONTROL LOOP. The first control loop is responsible for managing the current supplied to the transistor. This loop cannot address potential discontinuous state transitions and fails to guarantee a safe operating condition. In contrast, the secondary loop addresses these critical issues.

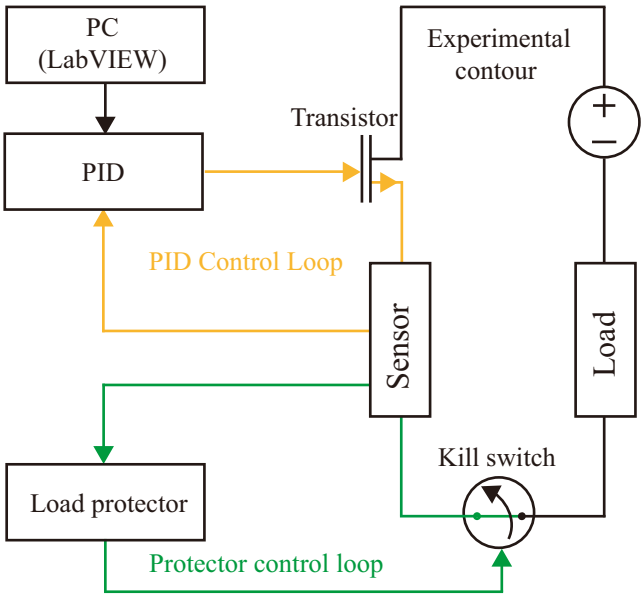


Fig. 1. Generic experiment control.

As illustrated in Fig. 2, the load current is maintained within the specified range I_a–I_b, and its activation time is accurately regulated by the duty cycle associated with the EMISSION and PROHIBITION periods. Following the EMISSION period, there exists a potential for the dispenser to be reactivated. The introduction of the PROHIBITION period eliminates this risk. It achieves this by preventing the automatic device from restarting prematurely, thereby keeping the average dissipated energy within an acceptable threshold range and ensuring system safety. To achieve a balance between heating and cooling, the working cycle needs to be adjusted according to the specific dynamics of the experiment. During the EMISSION stage, the following principles should be followed to optimize

the emission cycle: it should be consistent with the ideal heating and cooling times of the experiment, enabling rapid cycling without sacrificing the safety of the dispenser. The PROHIBITION period, activated sequentially after the EMISSION period, should be optional via a switch. The likely pulse operation involves a single chamber that must be cleared of gases before loading a new MOT. In our setup, the dispenser cools faster than the cycle time because of heat conduction through massive copper wires. Note that this may not be applicable to other configurations.

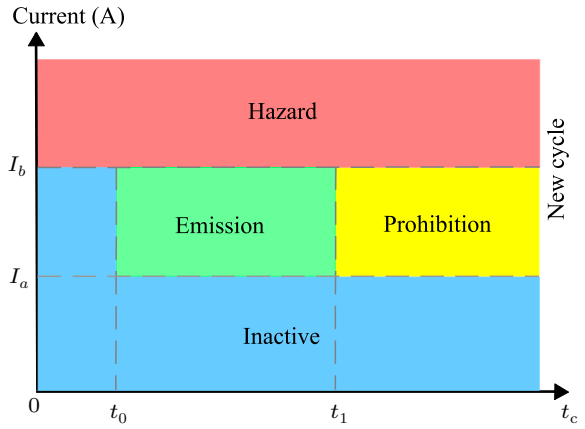


Fig. 2. Phase diagram of the evaporation range of Rb-dispenser.

Table 1 details the logical interconnections and operational parameters of the system shown in Fig. 2. The experimental protocol begins with the In1 Reset signal, which functions to reset all system variables and states, thereby ensuring a clearly defined initial condition. Subsequently, the start of the EMISSION state is indicated by the In2 EvapSt signal at time t_0, during which the load current is maintained within a designated safety threshold. It should be noted that t_0 experiences a delay, which is attributed to the thermal delay associated with heating the dispenser before the release of atoms. The EMISSION state represents the active period of atomic evaporation. At the end of this stage, the In3 Prohib signal terminates the EMISSION state and initiates the PROHIBITION state, thereby enabling precise adjustment of the duty cycle. Throughout the process, the In4 Fail signal continuously monitors the load current; if the current exceeds the preset threshold I_b, the system enters the HAZARD state as a protective measure. This logic output exhibits remarkable logical accuracy.

Specifically, the condition for the activation of the Out1 Alarm output is governed by the conjunction of the In4 Fail signal and the signal In1 Reset being false, as indicated by $\overline{\text{Reset}}$. This interrelationship is formally articulated as

$$\text{Alarm} = \text{Fail} \cdot \overline{\text{Reset}}. \tag{1}$$

The design logic substantially improves the reliability and safety of the system by ensuring that the alarm is activated exclusively upon the identification of a fault condition (Fail), contingent upon the system not being in a reset state ($\overline{\text{Reset}}$). This alarm remains activated until manually deactivated, ensuring that unnoticed faults are avoided and reducing the risk of undetected system failures during operation.

The activation of Out2 Evap is dependent upon more rigorous conditions, which involve the logical integration of four input signals. The corresponding expression is formulated as follows:

$$\text{Evap} = \overline{\text{Fail}} \cdot \overline{\text{Reset}} \cdot \text{EvapSt}\,(t = -\Delta t_1) \cdot \overline{\text{Prohib}}\,(t = -\Delta t_2), \tag{2}$$

where Evap signifies the initiation of the evaporation process. The EvapSt signal delineates the beginning of the EMISSION zone as depicted in Fig. 2, where its evaluation at $t = -\Delta t_1$ determines its duration. Analogously, Prohib marks the beginning of the PROHIBITION zone, with the term $t = -\Delta t_2$ determining its length. Therefore, the activation of the evaporation process is contingent upon: (i) the absence of any failure or reset, (ii) the prior initiation of the evaporation process at Δt_1, and (iii) the non-activation of the prohibition condition for Δt_2. This logical framework enforces strict conditions for initiating the evaporation process, ensuring compliance with safety and operational constraints.

Based on the logical framework of Table 1 and the dynamic time-electricity characteristics shown in Fig. 2, we present in Fig. 3 the functional representation of the operational behavior of the system. This figure provides the foundation for the actual implementation of the kill switch circuit system. The next section elaborates on the design and implementation of the circuits that execute the specified logical functions. We also emphasize the importance of selecting appropriate logic gates and optimizing their arrangement to ensure reliable performance and resource efficiency.

Table 1. Rb-dispenser protection circuit truth table.

Scenario No	In4 Fail	In3 Prohib	In2 EvapSt	In1 Reset	Out1 Alarm	Out2 Evap
1	0	0	0	0	0	0
2	0	0	0	1	0	0
3	0	0	1	0	0	1
4	0	0	1	1	0	0
5	0	1	0	0	0	0
6	0	1	0	1	0	0
7	0	1	1	0	0	0
8	0	1	1	1	0	0
9	1	0	0	0	1	0
10	1	0	0	1	0	0
11	1	0	1	0	1	0
12	1	0	1	1	0	0
13	1	1	0	0	1	0
14	1	1	0	1	0	0
15	1	1	1	0	1	0
16	1	1	1	1	0	0

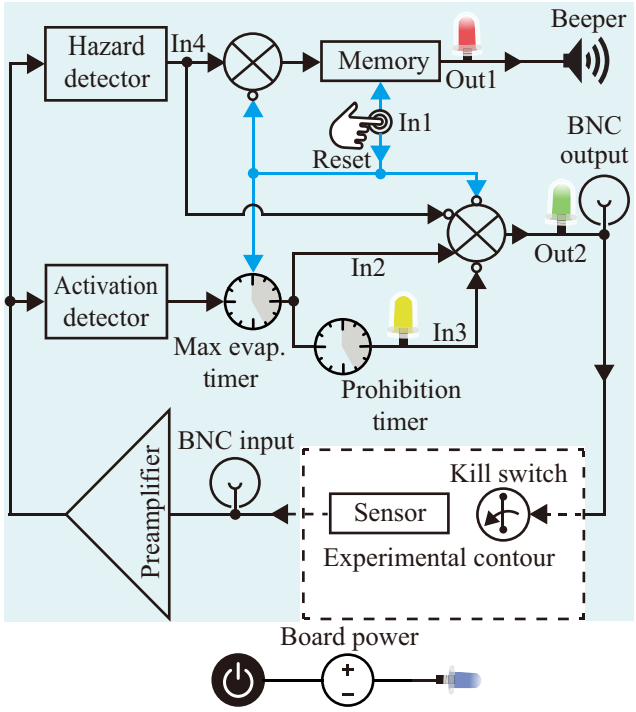


Fig. 3. Functional solution diagram. The light green background area corresponds to the LOAD PROTECTOR in Fig. 1. The LEDs are color-coded identically to the phase diagram in Fig. 2.

3. Circuit design

The detailed circuit schematic is shown in Fig. 4. Figure 5 shows the PCB (192 mm × 154 mm) designed with LTspice, housed in the aluminum enclosure shown in Fig. 6. The front panel has apertures for four LEDs and a reset function, while the rear panel contains power terminals, a ground port, and five adjustment holes for calibrating the PCB potentiometers, as shown in Fig. 7. The circuit bill of materials is listed in Table 2. The blue LED lights up, indicating that the PCB is powered on. The Reset signal originates from PWL (Piecewise Linear) high-level pulses controlled by LabVIEW. The SW_1 switch is used for manual reset. U1 inverts the Reset signal to create the not_reset signal, serving as an active-low reset for subsequent circuits. The sensor signal is transmitted to the preamplifier U2 through the potentiometer R1, which functions to optimize the operational range of the sensor. Upon integration of an INPUT, the circuit functions in two distinct modes as described below, where this parallel configuration effectively prevents potential competition or interference among signals.

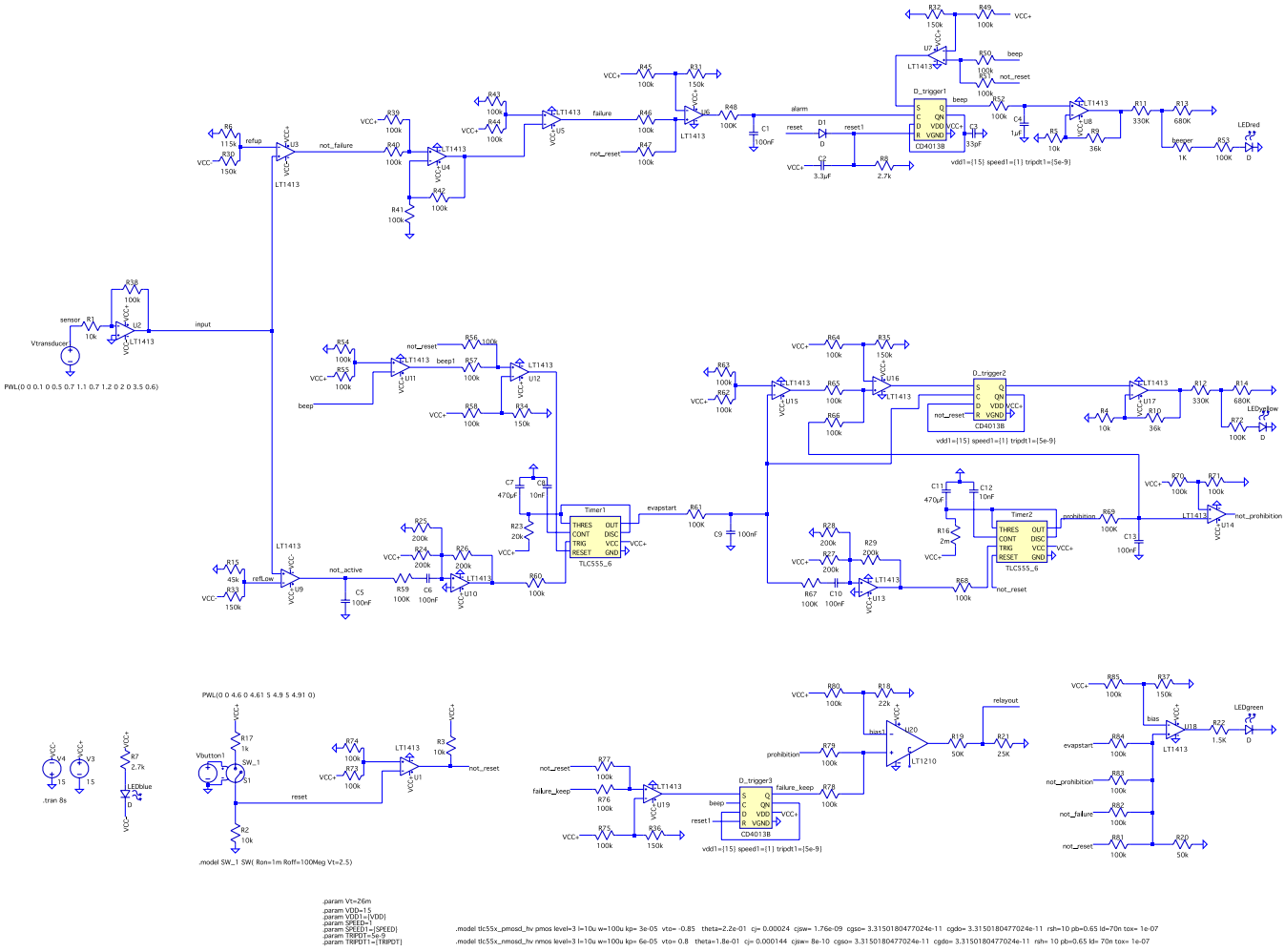


Fig. 4. The design circuit of the pre-emptive parametric kill switch.

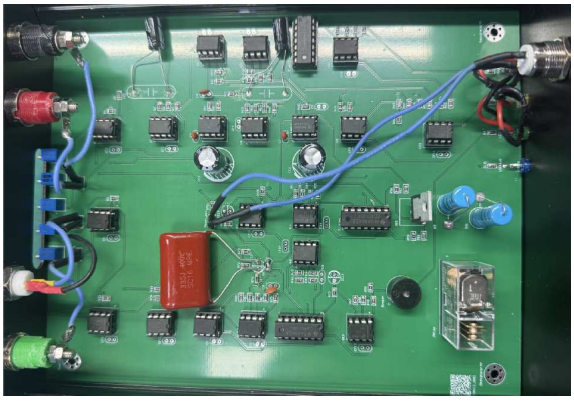


Fig. 5. PCB with dimensions of 192 mm × 154 mm, designed and verified in LTspice.



Fig. 6. Aluminum alloy enclosure (1.5 mm thickness, dimensions: 160 mm (L) × 192.6 mm (W) × 80 mm (H)) designed to house the PCB shown in Fig. 5, the front panel includes openings for four LED indicator lights and a reset button.

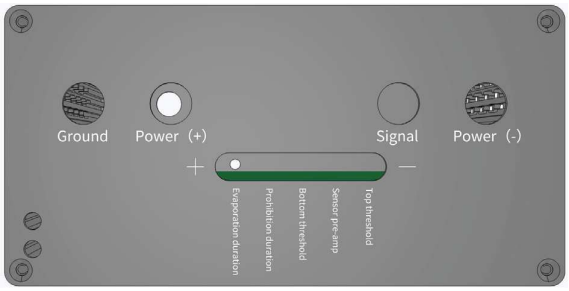


Fig. 7. Rear cover of the aluminum alloy enclosure in Fig. 6, featuring power input terminals, a ground port, and potentiometer adjustment holes.

One of the operation modes has an overcurrent alarm function. When the detected current exceeds the set upper limit I_b, the circuit issues an alarm to indicate that the current has risen abnormally. In this regard, the comparator U3 handles this task, with its reference level adjusted through the potentiometer R6. The output of U3, named not_failure, is then shaped by U4 together with the resistors R39–R42, which help to clean up the transitions and reduce the signal sensitivity to noise. The next stage, U5, simply inverts the logic and produces the active failure signal.

After that, U6 works as an AND gate, combining both failure and not_reset. The resulting signal passes through capacitor C1, which smooths it and eliminates bounce or short spikes, providing the final Alarm output as shown in Eq. (1). The Alarm signal acts as the clock input for D_trigger1. Meanwhile, the external reset line passes through the Zener diode D1, forming the internal node reset1. This node connects to the reset terminal of D_trigger1 and to the RC branch composed of C2 and R8, which performs the power reset. The diode D1 isolates the RC path, preventing stored charge from leaking back, while allowing the external reset function to operate normally.

The output from D_trigger1, named beep, passes through U8, which provides sufficient output current to reliably power both the buzzer and the red LED indicator (LEDred). Another part of the circuit processes the beep signal. Here, U7 performs the logical combination of beep and not_reset to generate the set input of D_trigger1, following:

$$\mathrm{S} = \mathrm{beep} \cdot \overline{\mathrm{Reset}}.$$

Consequently, this arrangement ensures that when the input voltage crosses the set limit, the alarm remains active until the system is manually reset. In this way, the circuit does not automatically recover when a fault occurs.

To prevent the dispenser from being mistakenly activated for an extended period due to faults or unexpected current fluctuations, the pre-emptive kill switch system incorporates a protection mechanism based on activation duration. This mechanism uses two internal timers to monitor the activation duration of the dispenser.

Specifically, the branch circuit incorporates a comparator U9 to detect the crossing of a predefined lower threshold I_a (the evaporation threshold). The reference voltage for U9 is established using the potentiometer R15. The U9 output signal is filtered by an RC circuit (R59, C3) to suppress noise and eliminate signal bounce, and is then compared with a 0 V reference by the comparator U10 to convert it into a stable digital logic signal.

This signal is input into the Timer1 module to set the dispenser activation duration (ΔT_1), where

$$\Delta T_1 \approx 1.1 \times C4 \times R23.$$

The R23 potentiometer provides a variable resistance to adjust the time constant. Module U11 modifies the beep signal to generate the beep1 signal, while module U12 combines beep1 with the not_reset signal to generate a stable control level, thereby driving the RESET pin of Timer1 and determining whether the timer operates or remains in the reset state. The Timer1 output is designated as evapstart.

To avoid the risk of unintended dispenser activation caused by transient pulse currents, the evapstart signal is split into two paths. The first path is processed by U13, which is configured with the same RC network components as U10 (R27–R29, R67, and C7), and then feeds Timer2, which sets the duration

$$\Delta T_2 \approx 1.1 \times C8 \times R16,$$

where R16 is implemented as a potentiometer. Its output, designated as prohibition, is inverted and shaped by U14 with peripheral resistors R70 and R71 to generate a stable NOT-prohibition signal. The second path routes the evapstart signal through U15 for signal conditioning and then combines it with prohibition in U16 before sending it to D_trigger2. This triggers U17, a buffer amplifier. The output activates LEDyellow, indicating that Timer2 is active.

This setup prevents prolonged activation states, thereby enhancing dispenser performance and extending its service life.

The final configuration of this circuit includes a four-input logic AND gate U18, which integrates the control signals evapstart, not_prohibition, not_failure, and not_reset to activate LEDgreen and the relay. The working principle of this gate is explained mathematically in Eq. (2). This method eliminates the need for additional driver chips, reduces the number of components, and decreases circuit board complexity while maintaining full functionality.

For gradual development convenience, one spare (unused) op-amp was retained in each dual-opamp chip.

Table 2. Bill of materials.

№	Part name	Manufacturer	Model ID	Tag	Characteristics	Packaging/Technology	Qty	USD/unit
1	Relay	Omron	G2R-1 DC5	-	5 V(DC), 10 A	SPDT	1	3.430
2	D-trigger	Texas Instruments	CD4013BE	Dtrigger	45 ns, 12 MHz, 3 V–18 V, 6.8 mA	PDIP-14	2	0.530
3	Timer	Texas Instruments	TLC555	Timer1, Timer2	5 V–15 V	PDIP-8	2	0.300
4	Operational Amplifier	Analog Devices	LT1413CN8#PBF	U1-19	950 kHz, 0.4 V/μs, ±2 V–±18 V	PDIP-8, 2 channels	17	6.420
5	Operational Amplifier	Analog Devices	LT1210CT7#PBF	U20	8 V–36 V, ±5 V–±15 V , 350 mA	TO-220, 1 channel	1	7.950
6	Beeper	Multicomp Pro	ABT-414-RC	beeper	3–8 V, 40 mA, 85 dB	–	1	1.050
7	LED	Broadcom	HLMP-3301	LEDRed	Red, 2.0–2.2 V, 20 mA	–	1	0.128
8	LED	Broadcom	HLMP-3401	LEDYellow	Yellow, 2.0–2.2 V, 20 mA	–	1	0.128
9	LED	Broadcom	HLMP-3507	LEDGreen	Green, 2.0–2.2 V,20 mA	–	1	0.128
10	LED	Broadcom	HLMP-LB65-RU0DD	LEDBlue	Blue, 3.0–3.2 V, 20 mA	–	1	0.497
11	Resistor	TE Connectivity	1622829-1	R2-5	10 kΩ, 50 V, 0.1 W	Surface Mount	4	0.007
12	Resistor	TE Connectivity	CRGCQ0402F2K7	R7,8	2.7 kΩ, 0.063 W	Surface Mount	2	0.007
13	Resistor	TE Connectivity	CRG0402F36K	R9,10	36 kΩ, 0.063 W	Surface Mount	2	0.007
14	Resistor	TE Connectivity	CRG0402F330K	R11,12	330 kΩ, 0.063 W	Surface Mount	2	0.007
15	Resistor	TE Connectivity	CRG0402F680K	R13,14	680 kΩ, 0.063 W	Surface Mount	2	0.004
16	Resistor	TE Connectivity	1-1622826-8	R17	1 kΩ, 0.5 W	Surface Mount	1	0.006
17	Resistor	TE Connectivity	CRGH2512J22K	R18	22 kΩ, 2 W, 200 V	Surface Mount	1	0.013
18	Resistor	Vishay	PNM0805E5002BST5	R19,20	50 kΩ, 0.2 W	Surface Mount	2	0.446
19	Resistor	TE Connectivity	AMP 1614911-6	R21	25 kΩ, 0.1 W	Surface Mount	1	0.129
20	Resistor	TE Connectivity	CRGCQ0402F1K5	R22	1.5 kΩ, 0.063 W	Surface Mount	1	0.006
21	Resistor	TE Connectivity	CRG0402F200K	R24-29	200 kΩ, 0.063 W	Surface Mount	4	0.003
22	Resistor	TE Connectivity	CRG0402F150K	R30-37	150 kΩ, 0.063 W	Surface Mount	5	0.006
23	Resistor	TE Connectivity	CRG0402F100K	R38-85	100 kΩ, 0.063 W	Surface Mount	11	0.007
24	Cermet trimmer potentiometer	Bournes	3296W-1-103LF	R1	10 kΩ, 0.5 W	25 turns, Cermet, THT	1	1.238
25	Cermet trimmer potentiometer	Bournes	3296W-1-204LF	R6	200 kΩ, 0.5 W	25 turns, Cermet, THT	1	1.192
26	Cermet trimmer potentiometer	Bournes	3296W-1-503LF	R15	50 kΩ, 0.5 W	25 turns, Cermet, THT	1	1.145
27	Cermet trimmer potentiometer	Bournes	3296W-1-205LF	R16	2 MΩ, 0.5 W	25 turns, Cermet, THT	1	1.190
28	Cermet trimmer potentiometer	Bournes	3299Y-1-203LF	R23	20 kΩ, 0.5 W	25 turns, Cermet, THT	1	1.470
29	Silicon Rectifier Diode	NTE Electronics	NTE507	D1	1 A, 50 V	Through Hole	1	0.675
30	Multilayer Ceramic Capacitor	Vishay	K103K15X7RH53L2	C5,C9	10 nF, 100 V	Radial Leaded	2	0.079
31	Plastic Film Capacitor	Panasonic	ECWFD2W335	C2	3.3 μF, 400 V	Radial Leaded	1	0.399
32	Multilayer Ceramic Capacitor	Vishay	K104K20X7RH5TL2	C1,C6	100 nF, 100 V	Radial Leaded	2	0.137
33	Aluminum Electrolytic Capacitor	Panasonic	EEUTA1C471	C4,C8	470 μF	Radial Leaded	2	0.484
34	Aluminum Electrolytic Capacitor	Panasonic	ECA2DHG470	C3,C7	47 μF	Radial Leaded	2	0.024
35	DIP Socket	TE Connectivity	1-2199298-2	–	1 A,250 V	8P	19	0.103
36	DIP Socket	SparkFun Electronics	PRT-07939	–	–	14P	3	0.600
37	Banana Jack	Cinch Connectivity Solutions	108-0903-001	–	15 A, 7 kVDC	Female	3	0.710
38	Pushbutton	Adam Tech	SW-PB1-1DZ-A-P1-A	SW_1	3 A, 250 V	solder type	1	0.235
39	PCB	Phoenix Contact	UM-BASIC 108/32 DEV-PCB	–	10 cm × 7 cm	–	1	0.505
40	PCB-mounting screws	–	–	–	$L = 25$ mm, $D = 3.2$ mm	–	4	0.150
41	Aluminum alloy enclosure	–	–	–	160 mm × 192.6 mm × 80 mm	1.5 mm thickness	1	18.860
							Total	**160.18**

To verify the fabricated board, we conducted bench-top functional tests on the fabricated circuit using a 1 Ω cement resistor as a substitute load instead of the dispenser. The experimental results confirmed the correct implementation of the primary board-level logic, including power status indication, initiation of the evaporation sequence, enforcement of prohibition timing, alarm activation, and manual reset functionality. At this stage, the results should be regarded as a board-level functional demonstration rather than a long-term validation in a fully integrated vacuum experimental system.

4. Summary and conclusions

In this work, we developed a protection circuit that proved reliable in practical operation, particularly for cold-atom ex-

periments. The primary purpose was to maintain the dispenser current within a safe region (I_a–I_b) and prevent accidental triggering caused by noise or sudden pulses. To achieve this, the circuit uses duty-cycle timing control: it only allows emission during ΔT_1 and automatically cuts off the current during the subsequent period ΔT_2. This simple modification makes the whole setup much safer by preventing overheating and extending the lifetime of the dispenser. Instead of using digital logic or a controller, we kept the entire design analog. While this may seem "old-fashioned", it eliminates potential failures associated with complex protection schemes in computer- or controller-based implementations, which may suffer from hanging or glitches caused by signal races. All components of the circuit are standard and inexpensive, making it easy to reproduce or repair. This makes the design highly practical for university laboratories or other small experimental setups. Our design may be applied to many other devices that share similar thermal or current-safety concerns — such as heater filaments, titanium sublimation pumps, or tungsten lamps. With a few adjustments, this protection logic could even be scaled up to larger applications, such as battery modules or high-power reactors, where early system shutdown can prevent much more serious failures.

Data availability

The circuit design files and the demonstration video can be obtained from GitHub repository.

Acknowledgments

Project supported by the SMEC Scientific Research Innovation Project (Grant No. 2023ZKZD55), the National Natural Science Foundation of China (Grant No. 92576102), the Science and Technology Commission of Shanghai Municipality (Grant No. 22ZR1444600), the NYU Shanghai Boost Fund, the China Foreign Experts Program (Grant No. G2021013002L), the NYU-ECNU Institute of Physics at NYU Shanghai, the NYU Shanghai Major-Grants Seed Fund, and Tamkeen under the NYU Abu Dhabi Research Institute (Grant No. CG008).

References

[1] Filzinger M, Caddell A R, Jani D, Steinel M, Giani L, Huntemann N and Roberts B M 2025 *Phys. Rev. Lett.* **134** 031001
[2] Nichol B, Srinivas R, Nadlinger D, Drmota P, Main D, Araneda G, Ballance C and Lucas D 2022 *Nature* **609** 689
[3] Cassens C, Meyer-Hoppe B, Rasel E and Klempt C 2025 *Phys. Rev. X* **15** 011029
[4] Szigeti S S, Nolan S P, Close J D and Haine S A 2020 *Phys. Rev. Lett.* **125** 100402
[5] Ladd T D, Jelezko F, Laflamme R, Nakamura Y, Monroe C and O'Brien J L 2010 *Nature* **464** 45
[6] De Leon N P, Itoh K M, Kim D, Mehta K K, Northup T E, Paik H, Palmer B, Samarth N, Sangtawesin S and Steuerman D W 2021 *Science* **372** eabb2823
[7] Wei B, Crawford A, Andeweg Y, Zhuo L, Li C and Raman C 2022 *Appl. Phys. Lett.* **120** 144011
[8] Martinez G D, Li C, Staron A, Kitching J, Raman C and McGehee W R 2023 *Nat. Commun.* **14** 3501
[9] Rusimova K R, Slavov D, Pradaux-Caggiano F, Collins J T, Gordeev S N, Carbery D R, Wadsworth W J, Mosley P J and Valev V K 2019 *Nat. Commun.* **10** 2328
[10] Millerioux Y, Touahri D, Hilico L, Clairon A, Felder R, Biraben F and de Beauvoir B 1994 *Opt. Commun.* **108** 91
[11] Matthews M, Hall D, Jin D, Ensher J, Wieman C, Cornell E A, Dalfovo F, Minniti C and Stringari S 1998 *Phys. Rev. Lett.* **81** 243
[12] Dugrain V, Rosenbusch P and Reichel J 2014 *Rev. Sci. Instrum.* **85** 083112
[13] Barker D S, Norrgard E B, Klimov N N, Fedchak J A, Scherschligt J and Eckel S 2019 *Phys. Rev. Appl.* **11** 064023
[14] Ivannikov V and Sidorov A I 2018 *J. Phys. B: At. Mol. Opt. Phys.* **51** 205002
[15] Ivannikov V 2013 *Analysis of a Trapped Atom Clock with Losses* (Ph.D. Thesis) (Swinburne: University of Technology)
[16] Kang S, Mott R P, Mis A V, Roper C S, Donley E A and Kitching J 2018 *Opt. Express* **26** 3696
[17] Christaller F, Mäusezahl M, Moumtsilis F, Belz A, Kübler H, Alaeian H, Adams C S, Löw R and Pfau T 2022 *Phys. Rev. Lett.* **128** 173401
[18] Karaulanov T, Graf M, English D, Rochester S, Rosen Y, Tsigutkin K, Budker D, Alexandrov E, Balabas M, Kimball D J, Narducci F, Pustelny S and Yashchuk V 2009 *Phys. Rev. A* **79** 012902
[19] Hänsel W, Hommelhoff P, Hänsch T and Reichel J 2001 *Nature* **413** 498
[20] Klempt C, Van Zoest T, Henninger T, Rasel E, Ertmer W and Arlt J 2006 *Phys. Rev. A* **73** 013410
[21] Gozzini A, Mango F, Xu J, Alzetta G, Maccarrone F and Bernheim R 1993 *Il Nuovo Cimento D* **15** 709
[22] Villalba S, Failache H and Lezama A 2010 *Phys. Rev. A* **81** 032901
[23] Kang S, Mott R P, Gilmore K A, Sorenson L D, Rakher M T, Donley E A, Kitching J and Roper C S 2017 *Appl. Phys. Lett.* **110** 244101
[24] McGilligan J, Moore K, Kang S, Mott R, Mis A, Roper C, Donley E and Kitching J 2020 *Phys. Rev. Appl.* **13** 044038
[25] Rapol U D, Wasan A and Natarajan V 2001 *Phys. Rev. A* **64** 023402
[26] Slowe C, Vernac L and Hau L V 2005 *Rev. Sci. Instrum.* **76** 103101
[27] Talker E, Arora P, Zektzer R, Sebbag Y, Dikopltsev M and Levy U 2021 *Phys. Rev. Appl.* **15** L051001
[28] Scherer D R, Fenner D B and Hensley J M 2012 *J. Vac. Sci. Technol. A* **30** 061602
[29] Sushkov A and Budker D 2008 *Phys. Rev. A* **77** 042707
[30] Plekhotkin G A 1983 *Obtaining the Vapours and Determining the Atomic Decay Constants of Zr, Nb, Mo, Ta, and W* (Ph.D. Thesis) (Leningrad State University originally) (in Russian)
[31] Kang S, Moore K R, McGilligan J P, Mott R, Mis A, Roper C, Donley E A and Kitching J 2019 *Opt. Lett.* **44** 3002
[32] Engler H, Weber T, Mudrich M, Grimm R and Weidemüller M 2000 *Phys. Rev. A* **62** 031402
[33] Ott H, Fortagh J, Schlotterbeck G, Grossmann A and Zimmermann C 2001 *Phys. Rev. Lett.* **87** 230401
[34] Succi M, Canino R and Ferrario B 1985 *Vacuum* **35** 579
[35] Li S, Tekin Z, Fan L, Li S, Zhang F, Ahmad S, Lin Z, Zhang M, Liu X T, Hu J, Yang D, Yang W, Radhakrishnan C, Byrnes T and Ivannikov V 2026 *AIP Adv.* **16** 035118
[36] Chen Y 2022 *Ionics* **28** 495
[37] Bekhti M, Bensaada M and Beldjehem M 2020 *Aeronaut. J.* **124** 1789
[38] Cui Y, Shi D, Wang Z, Mou L, Ou M, Fan T, Bi S, Zhang X, Yu Z and Fang Y 2023 *Batteries* **9** 438
[39] Xu W, Zhou K, Wang H, Lu L, Wu Y, Gao B, Shi C, Rui X, Wu X and Li Y 2024 *Energy* **308** 132999